Title

Interaction Forces between Lipid Rafts

Journal

Langmuir, 33(1)

ISSN

0743-7463

Authors

Kurniawan, James
Ventrici, João
Kittleson, Gregory
et al.

Publication Date

2017-01-10

DOI

10.1021/acs.langmuir.6b03717

Peer reviewed

Interaction Forces between Lipid Rafts

James Kurniawan[†], João Ventrici[‡], Gregory Kittleson[†] and Tonya L. Kuhl[†#]*

[†]Department of Chemical Engineering, University of California Davis, 95616, USA

[‡]Department of Chemistry, University of California Davis, 95616, USA

[#]Department of Biomedical Engineering, University of California Davis, 95616, USA

ABSTRACT: Cellular membranes containing sphingolipids and cholesterol have been shown to self-organize into lipid rafts, specialized domains which host integral membrane proteins and modulate the bioactivity of cells. In this work, force-distance profiles between raft membranes in the liquid ordered phase consisting of singly-unsaturated 1-palmitoyl-2-oleoyl-*sn*-glycero-3-phosphocholine (POPC), a complex mixture of brain sphingomyelin (BSM), and cholesterol were measured using the surface force apparatus (SFA). Two distinct force profiles were detected corresponding to uniform raft membranes and raft membranes with a higher level of topological membrane defects (heterogeneous) as corroborated by AFM scans. In all cases a weak, long-range electrostatic repulsion was observed with some variation in the surface charge density. The variation in electrostatic repulsion was attributed to charged lipid species primarily from the constituent lipids in the BSM mixture. The adhesion between the uniform raft membranes was comparable to our previous work with pure component, liquid-ordered POPC:DPPC (1,2-dipalmitoyl-*sn*-glycero-3-phosphocholine):cholesterol membranes. Raft membranes with more topological defects adhered more strongly due to hydrophobic attraction between exposed acyl chains. Even though the rafts were in the liquid-ordered phase and membrane defects were present in the contact region, the raft membranes were stable and no structural rearrangement was observed throughout the measurements. Our findings demonstrate that liquid ordered membranes are stable to mechanical loading and not particularly sensitive to compositional variation.

Keywords: brain sphingomyelin, POPC, cholesterol, supported lipid membrane, SFA, AFM

INTRODUCTION

Biological membranes are sophisticated structures that provide boundaries between discrete volumes in all life forms. They are composed of a myriad of different molecular species including various lipids, sterols, and proteins. These constituents are thought to segregate dynamically into nanoscale lateral domains called lipid rafts, which influence vital bioactivity such as signaling events, transport across biological membranes, and regulation of the activity of membrane proteins.[1, 2, 3, 4, 5] Due to the complexity of cell membranes, numerous studies have mimicked raft domain properties and phase state using simple model systems comprised of a high melting point (T_M) lipid, a low T_M lipid, and sterol.[2, 6, 7, 8] Such ternary mixtures can form coexisting liquid ordered (L_o) / liquid disordered (L_d) phases analogous to liquid-liquid immiscibility in cellular membranes and raft formation.[9, 10, 11, 12] Ternary mixtures of sphingomyelin (SM), phosphatidylcholine (PC), and cholesterol in particular are similar to the predominant lipid species in the outer membrane leaflet of eukaryotic cells.[6, 13, 14, 15, 16, 17] Most investigations of ternary SM/PC/cholesterol mixtures have focused on the importance of lateral, molecular level interactions in nanodomain formation. For example, the immiscible L_o/L_d coexistence phases of ternary SM/PC/cholesterol mixtures were mapped by thermodynamic analysis of differential scanning calorimetry (DSC) scans and fluorescence resonance energy transfer (FRET) to construct the ternary phase diagram.[6, 7, 14] The mechanisms responsible for lipid raft stability and domain size have also been studied by small angle neutron scattering (SANS) coupled with Monte-Carlo simulations.[2]

Despite the plethora of research on these more biologically relevant systems, little is known about intermembrane interactions between ternary mixed membranes containing SM, PC

and cholesterol that purportedly better mimic native lipid rafts. BSM is a natural complex mixture of sphingolipids and contains at least 6 different SM lipid species. The major lipid acyl chains are octadecanoyl (18:0) and nervonoyl (24:1). Biophysical studies of membranes containing more complex mixtures are becoming more common. Previous nuclear magnetic resonance (NMR) and molecular dynamic simulation studies have proposed that the variety in saturation and length of the SM amide-linked acyl chains mediate coupling between membrane leaflets through interdigitation of the long amide-linked acyl chain with the inner cytoplasmic leaflet.[18, 19, 20] In addition, the mismatch of acyl chain length has been suggested to hold an important role in the regulation of membrane protein partitioning in cellular membranes.[5, 19, 21] In this work, we measured the interactions between lipid raft membranes composed of BSM, POPC and cholesterol. The composition was selected due to their abundance in the outer leaflet of plasma membranes and greater relevance to biological systems.[22, 23] The resulting SFA force-distance profiles were corroborated with high-resolution AFM topography scans to reveal the contributions of van der Waals, electrostatic, hydration, and hydrophobic interactions. Due to its importance in controlling various cellular functions and bioactivity of cells, a more fundamental understanding of raft membranes is crucial. This work provides direct measurements of intermembrane interactions in this complex system.

MATERIALS AND METHODS

Chemicals. 1,2-dihexadecanoyl-*sn*-glycero-3-phosphoethanolamine (DPPE, melting point, T_M = 63 °C), 1-palmitoyl-2-oleoyl-*sn*-glycero-3-phosphocholine (POPC, T_M = -2 °C), N-(octadecanoyl)-sphing-4-enine-1-phosphocholine (BSM porcine brain, T_M = ~45 °C) and cholesterol (ovine wool, >98%, T_M = 148 °C) were purchased from Avanti Polar Lipids, Inc.

(Alabaster, AL) and used as received. BSM is a mixture of various acyl chain length: 50% 18:0, 21% 24:1, 7% 22:0, 5% 20:0, 5% 24:0, 2% 16:0 SM and 10% unknown lipid species. Sodium nitrate ($NaNO_3$ 99.995%) was purchased from Sigma-Aldrich (St. Louis, MO). Water was purified with a MilliQ gradient water purification system to a resistivity of 18 MΩ·cm.

Sample Preparation. Asymmetric supported lipid bilayers on mica were used in the SFA and AFM studies. The membranes were constructed using Langmuir-Blodgett (LB) deposition (Nima Coventry, U.K.). Identical LB deposition parameters to the previous study of ternary POPC-DPPC-cholesterol were used in order to make direct comparison of the resulting membrane structure and interaction behavior.[24] The inner monolayer for all the experiments was DPPE deposited at 45 mN/m and a dipping speed of 1 mm/min. Previous studies have shown that under these conditions, DPPE forms an almost defect free, robust and strongly physisorbed monolayer on mica with a transfer ratio of 0.997 ± 0.004 [24] and thickness of 2.56 ± 0.05 nm.[25] The tight packing and stability of the gel phase DPPE inner monolayer minimizes molecular exchange between the inner and outer leaflets enabling asymmetric membrane leaflets to be studied. Moreover, this asymmetry mimics plasma membranes which are enriched in PE lipids on the cytoplasmic side and enriched in SM on the exoplasmic leaflet. The outer monolayer was 1:1:2 POPC-BSM-cholesterol LB deposited at 30 mN/m (average area per lipid of about 1/42 $Å^2$) and dipping speed of 4 mm/min under low-oxygen environment (<1 vol% O_2). The transfer ratio of the outer monolayer was 0.995 ± 0.018. The deposition of the outer layer was performed within 30 minutes under inert nitrogen or argon gas to minimize oxidation of cholesterol and lipid components. After lipid bilayer deposition, the surfaces were transferred underwater and mounted into the SFA.

Surface Force Measurements (SFA). The SFA technique has been used extensively to

measure the interaction forces between surfaces and details of the technique can be found in the following references.[26, 27, 28, 29] Based on multiple-beam interferometry (MBI), SFA provides an absolute measure of surface separation (±0.2 nm in this work). One of the membrane-coated mica surfaces was mounted on a fixed stage and the other on a vertically displaceable double cantilever spring of known stiffness (~2.8×10^5 mN/m). The back of the mica substrates was coated with a 55 nm thick, evaporated silver layer. The silver layer on each disk partially transmits light directed normally through the surfaces which constructively interferes producing fringes of equal chromatic order (FECO). The distance between the surfaces was measured by observation of the position and displacement of FECO peak wavelengths within a spectrometer. A custom automated SFA Mark-II was used for data collection.[30] The system enables constant and/or variable surface displacements via a computer-controlled motor system. A sensitive CCD camera (Princeton SPEC-10:2K Roper Scientific, Trenton, NJ) was interfaced with the spectrometer and computer acquisition system to allow automated FECO wavelength determination and accurate force-distance profiles to be measured.

The subphase in the SFA was 0.5 mM $NaNO_3$ solution and saturated with lipids to minimize lipid desorption from the surface during the course of the measurements. After the surfaces were mounted, the SFA was placed in a temperature-controlled room at 25.0 °C for at least two hours to equilibrate. The membrane thickness was determined using the FECO wavelength shift from membrane contact relative to bare mica substrates after completing each experiment.[25, 31] As the membranes were asymmetric, with inner leaflets of DPPE and outer leaflets of POPC-BSM-cholesterol mixtures, we treated the two outer leaflets, which we are primarily interested in, as an equivalent membrane of the mixture composition. Force profiles shown in the results section are representative force-distance profiles of seven independent

experiments. The force profiles shown are typical for experiments with uniform, low levels of topological membrane defects and heterogeneous lipid raft membranes with a higher defect density. At least five repeatable force measurements were taken for each independent experiment. The reported error propagation in the results section was based on the average of the five force runs for each independent measurement and showed the range of the observed experimental parameters for the two different conditions. Two additional independent SFA experiments were carried out to determine the thickness of a 1:1:2 POPC-BSM-cholesterol monolayer on mica. These measurements in air were used to determine the "dry" thickness of a POPC-BSM-cholesterol monolayer and quantify the hydration between the 1:1:2 POPC-BSM-cholesterol raft membranes in water.

Atomic Force Microscopy (AFM). AFM images were acquired using an MFP3D-SA system (Asylum Research, Santa Barbara, CA). A silicon cantilever (model MSNL-10, Bruker, Santa Barbara, CA) with force constant of 0.6 N/m was used for imaging. All the images were acquired in contact mode with a force of 12 nN. AFM images were analyzed using Gwyddion Version 2.31 (http://gwyddion.net/).

RESULTS

Force – distance profiles. The measured force profiles between opposing 1:1:2 POPC-BSM-cholesterol lipid raft membranes are shown in Figure 1. Seven independent experiments were carried out and two distinct force profiles were observed. The force-distance profiles shown using the square and diamond symbols were from experiments with uniform (low defect) lipid raft membranes. In this case, the equivalent membrane thickness of the two outer raft monolayer leaflets including hydration was 6.5±0.2 nm. A weak, long-range electrostatic repulsion with

decay length consistent with the electrolyte concentration (0.5 mM $NaNO_3$) was observed. The electrostatic repulsion was fitted to the non-linearized Poisson-Boltzmann equation, yielding a range of constant surface charge densities from 2.6±0.6 to 4.3±0.4 mC/m^2 or surface potentials between 25±6 and 43±4 mV for the various experiments. Based on an average area per molecule of 1/42 Å^2 and that cholesterol was uncharged, these charge densities indicate that 1.3 to 2.3% of the lipids were charged in the outer leaflet of the raft membrane. Although there was variation in the electrostatic repulsion between independent experiments, the electrostatic repulsion for a given membrane contacting region was reproducible. It was therefore straightforward to fit the electrostatic contribution to the measured force profile for a given series of measurements. As the electrostatic and van der Waals attraction should be additive, the electrostatic interaction was subtracted from the total force profile to deduce the attractive component of the membrane raft – membrane raft interaction. After removing the electrostatic contribution, the magnitude of the adhesion between the more uniform lipid rafts ranged between 1.3±0.2 and 1.5±0.2 mN/m.

The force-distance profile of more heterogeneous (higher defect density) lipid rafts are shown as triangles in Figure 1. In these cases, the equivalent membrane thickness of the two outer raft monolayers was less, 5.7±0.2 nm, consistent with a lower packing and topological defects (depressions) in the membrane. As with the uniform bilayers, electrostatic repulsion was observed with the decay length consistent with the electrolyte concentration. A higher constant surface charge density ranging from 4.5±0.5 to 5.9±0.6 mC/m^2, or a constant surface potential between 60±5 and 70±5 mV, was found for the more heterogeneous raft membranes. This level of charge density indicates 2.4 to 3.0% of the lipids in the outer leaflet were charged. After subtracting the electrostatic contribution, a higher magnitude of adhesion between 3.8±0.2 to 4.3±0.2 mN/m was apparent.

With both uniform and more heterogeneous lipid raft membranes, some variation in the electrostatic repulsion was observed. Even though POPC-BSM-cholesterol mixtures are usually considered to be ternary, BSM itself is a mixture of more than 6 different sphingolipids with saturated 18:0 SM as the major constituent in the mixture (~50%). Indeed, 10% of the BSM is unidentified lipid. We hypothesize that the experimental variations between ostensibly identical raft membranes was due to subtle differences in the molecular concentrations of charged lipid species. Moreover, a number of recent papers have found lipid membranes composed of purportedly overall neutral lipid species to be charged systems.[24, 31, 32, 33] In comparison, raft membranes made of pure liquid-ordered 1:1:1 POPC-DPPC-cholesterol membranes only a small level of charge was found, and there was little to no variation in the adhesion or electrostatic repulsion in the measured interaction force profiles.[24] The consistency in the force-distance profiles in this case was attributed to the higher purity and more uniform composition, while more physiological lipid rafts containing a complex, natural BSM composition show more variation.

Adhesion magnitude and presence of topological membrane defects. A significant difference in membrane adhesion was found between the more uniform and heterogeneous lipid raft membranes. High-resolution AFM scans of the raft membranes (Figure 2) revealed the presence of variable-sized nanoscopic topological defects in the outer membrane leaflet that reached the underlying inner leaflet. Most of the defects were below a few hundred nanometers in diameter. In a few cases with the heterogeneous membranes, defects about a micron in diameter were detected. Based on a typical contact area of ~35 μm^2 for the SFA measurements, the defect density across the samples varied between 0.5 to 8%. Hence, only a small variation in the adhesion was found for uniform raft membranes, which also had a correspondingly larger

membrane thickness. In contrast, the higher adhesion in the more heterogeneous raft membranes was attributed to additional hydrophobic attraction due to exposed acyl chains in the contact region. The reference frame for $D = 0$ in the force profiles (Figure 1) is contact between bare mica substrates and therefore corresponds to the total thicknesses of the two opposing membranes. At a small applied force of 1 mN/m, the combined uniform and heterogeneous raft membranes thicknesses were 11.9±0.3 and 11.1±0.3 nm, respectively. For comparison, the AFM was used to obtain the membrane thickness by "shaving" away the inner DPPE monolayer leaflet in one of the large micron sized defects. The total thickness of about 6 nm, or equivalently 12 nm for two membranes, is consistent with that measured by SFA. Importantly, the contact mode AFM scans were stable and no change in defect shape was observed when scanning. Similar stability behavior was observed for pure component liquid-ordered 1:1:1 POPC-DPPC-cholesterol membranes. Likewise, no structural rearrangement was observed throughout the SFA experiments even though the raft membranes were in the liquid-ordered phase and membrane defects were present in the contact region. In addition, the adhesion magnitude of the pure system was comparable, as well[24], to the uniform raft membranes.

Equivalent thickness and hydration of raft membranes. The equivalent raft membranes thickness was defined as the thickness of the two outer monolayers including their water of hydration. The equivalent thicknesses of the raft membranes were 6.5±0.2 and 5.7±0.2 nm for the uniform and heterogeneous membranes, respectively. In order to determine the thickness of the hydration layer between the raft membranes, two independent measurements of raft monolayers on mica in air were carried out. The dry monolayer thickness was 2.2±0.1 nm. With this value, the hydration layer is 2.1±0.3 nm (6.5 nm minus two dry monolayers) for well-packed, uniform raft membranes, which is comparable to a previous study by Marra and

Israelachvili on hydration between pure PC bilayers.[28]

DISCUSSION

The primary goal of this work was to obtain a better understanding of properties and interactions between lipid raft membranes in a more complex biomimetic system. Asymmetric membrane leaflets were used to better mimic plasma membranes which are enriched in PE lipids on the cytoplasmic side and enriched in SM on the exoplasmic leaflet. A composition of 1:1:2 BSM-POPC-cholesterol was selected for the outer leaflet to ensure the raft membrane was in the L_o phase and thus comparisons could be made to our previous work of pure component L_o ternary mixtures of DPPC-POPC-cholesterol without the complication of phase separation. BSM is a complex mixture of sphingolipids with a variety of amide-linked acyl chain lengths. Studies have suggested that the long chained SM lipids in the outer membrane leaflet might interdigitate and affect the overall structure or phase state of the bilayer membrane.[19, 20, 34, 35] For example, fluorescence experiments of asymmetric bilayers indicated that domains on the outer leaflet and the coupling between the membrane leaflets can induce formation of domains in the inner leaflet.[23, 36] In this work, the raft membrane mixture of 1:1:2 BSM-POPC-cholesterol was deposited onto an almost defect-free, gel phase DPPE monolayer immobilized on mica. Phase separation or formation of nanodomains was not observed by high-resolution AFM topography scans and confirmed that the raft membranes existed as a single L_o phase. Consequently, the preferential interaction between some sphingolipid species with various hydrophobic chain lengths and other components in the membrane was negligible or not discernible by high resolution AFM scans for this composition.[2] Likewise, no evidence of interdigitation of the long amide-linked acyl chain SM lipid between the leaflets was detected.

The observed behavior of these more biological low defect density (uniform) raft membranes revealed similar properties to well-studied pure component systems. In terms of adhesion magnitude, the uniform well-packed raft membranes had comparable van der Waals attraction (1.3±0.2 to 1.5±0.2 mN/m) to the ternary mixed membranes containing pure DPPC (1.8±0.2 mN/m).[24] The adhesion of these L_o supported membranes was higher than previously measured values for fluid and gel phase PC membranes (0.5-1.0 mN/m)[28, 37, 38] and significantly lower than adhesion between gel phase PE membranes (5-6 mN/m).[28] Both PC and PE membranes are expected to have similar Hamaker constants based on their structure and previous SFA[28] and refractive index measurements.[25] Thus, the differences in the measured adhesion between the ternary L_o phase membranes can be attributed to the variation in the lipid composition, contact separation and hydration thickness between the membranes. Even though the adhesion magnitude is similar in both L_o systems, the more biological raft membrane equivalent thickness was lower compared to the thickness of pure lipid 1:1:1 ternary mixed membranes. The main difference between the two systems was the saturated lipid component in the ternary mixture (BSM *vs.* DPPC). In comparison to glycerol lipids, SM can both hydrogen bond donate and accept. This difference in intermolecular hydrogen bonding structure could account for the reduced hydration and thinner equivalent thickness of the BSM raft membranes.[19]

In both the uniform and heterogeneous raft membrane experiments, as well as in recent studies with supported lipid membranes of different lipid compositions, a small electrostatic repulsion has been observed.[24, 31, 32, 33] As reported previously, the electrostatic repulsion is due to a small fraction of charged lipid species in the membrane.[32, 33] AFM scans of our raft membranes revealed that membrane-spanning holes were not present. Thus, the measured charge was not due to the underlying mica support, further confirming that charged lipid species are the source of the

electrostatic repulsion. This conclusion is also consistent with the previously studied pure component 1:1:1 system.

Despite the dramatic difference in the cholesterol concentration (33 *vs.* 50 mole%) and high T_M lipid constituents, L_o membranes of different compositions had very similar interactions, compressibility and stability. Although cholesterol is known to fluidize membranes, biomimetic raft membranes in the L_o phase are highly stable and do not show structural rearrangements such as thinning or higher adhesion with increased contact time or load. This stability is surprising given the hypothesized fluctuations of lipid raft domains. Although domain size is highly dependent upon lipid composition, the uniformity in behavior of L_o membranes suggests that membrane phase state may be more important for predicting membrane properties than the actual lipid composition. Given that many cellular membranes have similar properties yet contain a wide array of different constituent molecules, the potential of phase state to capture membrane properties vs. composition is significant. Continued investigations with more biologically complex systems are needed to further address this issue.

CONCLUSION

This study determined the interaction behavior between liquid-ordered biomimetic lipid raft membranes composed of 1:1:2 POPC-BSM-cholesterol. The force-distance profiles showed representative interaction behavior between low defect density (uniform) and higher defect density (heterogeneous) raft membranes. The variety of sphingolipids in the raft membrane resulted in the presence of non-uniform sized nanoscopic membrane topological defects of densities varying between 0.5 to 8%. Variations in the long-range electrostatic repulsion and measured raft membrane adhesion were also attributed to the heterogeneity of the constituent

sphingolipids. In comparison, no variation in interaction behavior was observed in our previous work with liquid-ordered ternary mixtures of pure POPC-DPPC-cholesterol membranes. Nevertheless, these more complex raft membranes exhibited an adhesion magnitude and compressibility similar to the ternary mixed membranes containing pure components.[24] The similarity in behavior of liquid-ordered membranes indicates that their physical properties are not very sensitive to the molecular details of the saturated lipid species. The variation in acyl chain lengths and hydrogen bonding structure due to amide linkages and hydration shell of sphingolipids only led to subtle changes in the overall interaction forces in the liquid-ordered ternary membranes. The insensitivity in the interaction behavior over the range of components and compositions (*i.e*. the high concentration of cholesterol and complex mixture of BSM constituent lipids) suggests that membranes in liquid ordered phases may have well-defined properties. If cellular membranes rafts are liquid ordered phases, it may be possible to reasonably simulate their properties with synthetic mixtures and future studies may employ well-defined synthetic lipid membranes for various applications. Furthermore, these findings may reconcile why physiological membranes can have different compositions but similar behavior.

AUTHOR INFORMATION

Corresponding Author

*E-mail: tlkuhl@ucdavis.edu

Notes

The authors declare no competing financial interest.

ACKNOWLEDGMENTS

This work was supported by the NSF chemistry division through grant CHE-1413745. We thank

Shawn Mattathill for assistance with transfer ratio measurements.

REFERENCE

1. Lingwood, D.; Simons, K. Lipid Rafts As a Membrane-Organizing Principle. *Science* **2010,** *327* (5961), 46-50.
2. Petruzielo, R. S.; Heberle, F. A.; Drazba, P.; Katsaras, J.; Feigenson, G. W. Phase behavior and domain size in sphingomyelin-containing lipid bilayers. *Bba-Biomembranes* **2013,** *1828* (4), 1302-1313.
3. Dietrich, C.; Bagatolli, L. A.; Volovyk, Z. N.; Thompson, N. L.; Levi, M.; Jacobson, K.; Gratton, E. Lipid rafts reconstituted in model membranes. *Biophys J* **2001,** *80* (3), 1417-1428.
4. Brown, D. A.; London, E. Structure and function of sphingolipid- and cholesterol-rich membrane rafts. *J Biol Chem* **2000,** *275* (23), 17221-17224.
5. Simons, K.; Ikonen, E. Functional rafts in cell membranes. *Nature* **1997,** *387* (6633), 569-572.
6. Pokorny, A.; Yandek, L. E.; Elegbede, A. I.; Hinderliter, A.; Almeida, P. F. F. Temperature and composition dependence of the interaction of delta-lysin with ternary mixtures of sphingomyelin/cholesterol/POPC. *Biophys J* **2006,** *91* (6), 2184-2197.
7. Frazier, M. L.; Wright, J. R.; Pokorny, A.; Almeida, P. F. F. Investigation of domain formation in sphingomyelin/cholesterol/POPC mixtures by fluorescence resonance energy transfer and Monte Carlo simulations. *Biophys J* **2007,** *92* (7), 2422-2433.
8. Heberle, F. A.; Feigenson, G. W. Phase Separation in Lipid Membranes. *Csh Perspect Biol* **2011,** *3* (4).
9. Veatch, S. L.; Keller, S. L. Seeing spots: Complex phase behavior in simple membranes. *Bba-Mol Cell Res* **2005,** *1746* (3), 172-185.
10. Stottrup, B. L.; Veatch, S. L.; Keller, S. L. Nonequilibrium behavior in supported lipid membranes containing cholesterol. *Biophys J* **2004,** *86* (5), 2942-2950.
11. Stottrup, B. L.; Stevens, D. S.; Keller, S. L. Miscibility of ternary mixtures of phospholipids and cholesterol in monolayers, and application to bilayer systems. *Biophys J* **2005,** *88* (1), 269-276.
12. Schroeder, R.; London, E.; Brown, D. Interactions between Saturated Acyl Chains Confer Detergent Resistance on Lipids and Glycosylphosphatidylinositol (Gpi)-Anchored Proteins - Gpi-Anchored Proteins in Liposomes and Cells Show Similar Behavior. *P Natl Acad Sci USA* **1994,** *91* (25), 12130-12134.
13. Ahmed, S. N.; Brown, D. A.; London, E. On the origin of sphingolipid/cholesterol-rich detergent-insoluble cell membranes: Physiological concentrations of cholesterol and sphingolipid induce formation of a detergent-insoluble, liquid-ordered lipid phase in model membranes. *Biochemistry-Us* **1997,** *36* (36), 10944-10953.
14. de Almeida, R. F. M.; Fedorov, A.; Prieto, M. Sphingomyelin/phosphatidylcholine/cholesterol phase diagram: Boundaries and composition of lipid rafts. *Biophys J* **2003,** *85* (4), 2406-2416.
15. Barenholz, Y.; Thompson, T. E. Sphingomyelin: biophysical aspects. *Chem Phys Lipids* **1999,** *102* (1-2), 29-34.
16. Zachowski, A. Phospholipids in Animal Eukaryotic Membranes - Transverse Asymmetry and Movement. *Biochem J* **1993,** *294*, 1-14.
17. Crane, J. M.; Tamm, L. K. Role of cholesterol in the formation and nature of lipid rafts in

planar and spherical model membranes. *Biophys J* **2004,** *86* (5), 2965-2979.
18. Niemela, P. S.; Hyvonen, M. T.; Vattulainen, I. Influence of chain length and unsaturation on sphingomyelin bilayers. *Biophys J* **2006,** *90* (3), 851-863.
19. Niemela, P. S.; Hyvonen, M. T.; Vattulainen, I. Atom-scale molecular interactions in lipid raft mixtures. *Bba-Biomembranes* **2009,** *1788* (1), 122-135.
20. Schmidt, C. F.; Barenholz, Y.; Huang, C.; Thompson, T. E. Monolayer Coupling in Sphingomyelin Bilayer Systems. *Nature* **1978,** *271* (5647), 775-777.
21. Jensen, M. O.; Mouritsen, O. G. Lipids do influence protein function - the hydrophobic matching hypothesis revisited. *Bba-Biomembranes* **2004,** *1666* (1-2), 205-226.
22. Davey, J. Biomembranes - Molecular-Structure and Function - Gennis,Rb. *Nature* **1989,** *339* (6226), 591-591.
23. Kiessling, V.; Wan, C.; Tamm, L. K. Domain coupling in asymmetric lipid bilayers. *Bba-Biomembranes* **2009,** *1788* (1), 64-71.
24. Kurniawan, J.; Yin, N. N.; Liu, G. Y.; Kuhl, T. L. Interaction Forces between Ternary Lipid Bilayers Containing Cholesterol. *Langmuir* **2014,** *30* (17), 4997-5004.
25. Kienle, D. F.; de Souza, J. V.; Watkins, E. B.; Kuhl, T. L. Thickness and refractive index of DPPC and DPPE monolayers by multiple-beam interferometry. *Anal Bioanal Chem* **2014,** *406* (19), 4725-4733.
26. Israelachvili, J. N. Thin-Film Studies Using Multiple-Beam Interferometry. *J Colloid Interf Sci* **1973,** *44* (2), 259-272.
27. Israelachvili, J. N.; Adams, G. E. Measurement of Forces between 2 Mica Surfaces in Aqueous-Electrolyte Solutions in Range 0-100 Nm. *J Chem Soc Farad T 1* **1978,** *74*, 975-&.
28. Marra, J.; Israelachvili, J. Direct Measurements of Forces between Phosphatidylcholine and Phosphatidylethanolamine Bilayers in Aqueous-Electrolyte Solutions. *Biochemistry-Us* **1985,** *24* (17), 4608-4618.
29. Kuhl, T. L.; Leckband, D. E.; Lasic, D. D.; Israelachvili, J. N. Modulation of Interaction Forces between Bilayers Exposing Short-Chained Ethylene-Oxide Headgroups. *Biophys J* **1994,** *66* (5), 1479-1488.
30. Moore, N. W.; Mulder, D. J.; Kuhl, T. L. Adhesion from tethered ligand-receptor bonds with microsecond lifetimes. *Langmuir* **2008,** *24* (4), 1212-1218.
31. Kurniawan, J.; Kuhl, T. L. Characterization of Solid-Supported Dipalmitoylphosphatidylcholine Membranes Containing Cholesterol. *Langmuir* **2015,** *31* (8), 2527-2532.
32. Hemmerle, A.; Malaquin, L.; Charitat, T.; Lecuyer, S.; Fragneto, G.; Daillant, J. Controlling interactions in supported bilayers from weak electrostatic repulsion to high osmotic pressure. *P Natl Acad Sci USA* **2012,** *109* (49), 19938-19942.
33. Schrader, A. M.; Donaldson, S. H.; Song, J.; Cheng, C. Y.; Lee, D. W.; Han, S.; Israelachvili, J. N. Correlating steric hydration forces with water dynamics through surface force and diffusion NMR measurements in a lipid-DMSO-H2O system. *P Natl Acad Sci USA* **2015,** *112* (34), 10708-10713.
34. Huang, C. H.; Mason, J. T. Structure and Properties of Mixed-Chain Phospholipid Assemblies. *Biochim Biophys Acta* **1986,** *864* (3-4), 423-470.
35. Maulik, P. R.; Atkinson, D.; Shipley, G. G. X-Ray-Scattering of Vesicles of N-Acyl Sphingomyelins - Determination of Bilayer Thickness. *Biophys J* **1986,** *50* (6), 1071-1077.
36. Kiessling, V.; Crane, J. M.; Tamm, L. K. Transbilayer effects of raft-like lipid domains in asymmetric planar bilayers measured by single molecule tracking. *Biophys J* **2006,** *91* (9), 3313-

3326.
37. Kuhl, T.; Guo, Y. Q.; Alderfer, J. L.; Berman, A. D.; Leckband, D.; Israelachvili, J.; Hui, S. W. Direct measurement of polyethylene glycol induced depletion attraction between lipid bilayers. *Langmuir* **1996,** *12* (12), 3003-3014.
38. Orozco-Alcaraz, R.; Kuhl, T. L. Interaction Forces between DPPC Bilayers on Glass. *Langmuir* **2013,** *29* (1), 337-343.

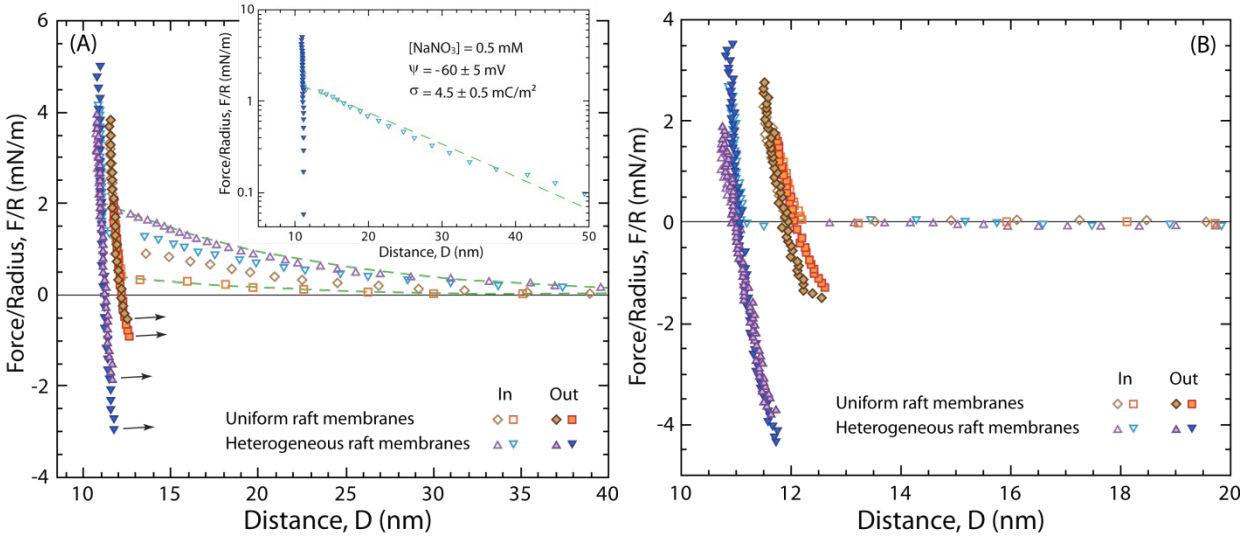

Figure 1. (A) Force–distance profiles between lipid raft membranes composed of 1:1:2 POPC-BSM-cholesterol membranes of two different thicknesses in 0.5 mM $NaNO_3$ solution were obtained (Diamond and square curves: uniform raft membranes; triangle and inverted triangle curves: heterogeneous raft membranes). Dashed lines represent the range of observed long-range electrostatic repulsion. Inset: an exemplar semi-logarithmic plot of a force profile and fit of the electrostatic contribution (dashed line) with origin of charge at the membrane surface. D = 0 is defined as the contact between bare mica–mica surfaces. (B) Force-distance profiles after subtraction of the electrostatic contribution. Open and filled symbols represent approach and separation respectively.

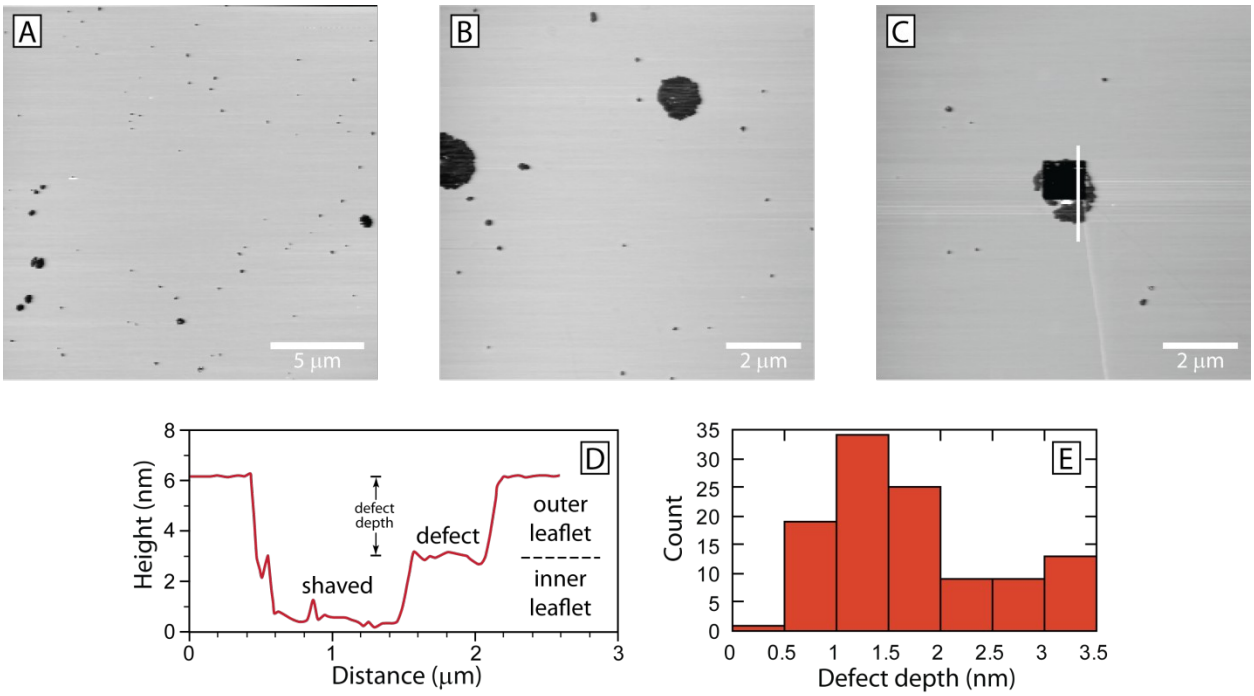

Figure 2. [A] Typical AFM topography scans of lipid raft membranes composed of 1:1:2 POPC-BSM-cholesterol in 0.5 mM $NaNO_3$ solution. [B] Scan of a membrane with micron diameter topological defects. [C] Membrane defect with diameter of ~1.5 µm. The center of the defect was removed or shaved off using the AFM tip. Removal of the inner leaflet in the defect allowed the total thickness of the membrane to be measured. [D] The corresponding cursor profile (vertical line on [C]) is shown. [E] Histogram of the defect depths over four independent samples with at

least five scans per sample.

Table 1. Summary of SFA results showing the ranges of various extracted parameters.

Lipid Raft Membrane	Equivalent Thickness (nm)*	σ (mC/m^2)	Ψ (mV)	F_{ad}/R (mN/m)	$\lvert F_{ad}/R \rvert$** (mN/m)
Uniform (low defect density)	6.5±0.2	2.6±0.6 to 4.3±0.4	25±6 to 43±4	-0.5±0.2 to -0.9±0.2	1.3±0.2 to 1.5±0.2
Heterogeneous (higher defect density)	5.7±0.2	4.5±0.5 to 5.9±0.6	60±5 to 70±5	-1.8±0.2 to -3.0±0.2	3.8±0.2 to 4.3±0.2

* The equivalent thickness is the thickness of the two outer monolayers including their hydration layer
** Effective adhesion after subtraction of the electrostatic contribution to the measured interaction force profile.

Table of Content Figure